Journal of Theoretical Biology 444 (2018) 38–49

Contents lists available at ScienceDirect

Journal of Theoretical Biology

journal homepage: www.elsevier.com/locate/jtbi

Thermal actuation in TRPV1: Role of embedded lipids and intracellular domains

Corey Melnick*, Massoud Kaviany

University of Michigan Department of Mechanical Engineering, Heat Transfer Physics Laboratory, Ann Arbor, MI 48105, United States

ARTICLE INFO

Article history:
Received 7 September 2017
Revised 29 January 2018
Accepted 1 February 2018
Available online 6 February 2018

Keywords:
Membrane protein
Thermosensation
Ion channel
Transient receptor potential

ABSTRACT

The transient response potential cation channel TRPV1 responds to high temperature, but many of the mechanisms driving its thermal actuation remain unclear. Its recently resolved structure has enabled a number of molecular dynamics (MD) studies focused on illuminating these mechanisms. We add to these efforts by performing the first all-atom MD simulations of its most recently resolved structure at different temperatures. While the complete, thermally induced transition of TRPV1 from its closed to open configuration remains elusive, our analysis of the hydrogen bonding networks, thermodynamics, hydration, and principal components of motion provide a wealth of information on the mechanisms which initiate or influence the thermal opening in TRPV1. In particular, we (i) support the previously proposed mechanism driving thermal actuation in the extracellular pore of TRPV1, (ii) present new hypotheses regarding the thermal actuation in the C-terminal and adjacent linker domains, and (iii) support and build upon the existing hypothesis regarding the role of the vanilloid binding pocket and lipids embedded therein.

1. Introduction

The transient receptor potential (TRP) ion channels are known for their ability to sense a variety of stimuli (Clapham, 2003; Voets et al., 2005), including hot (Caterina et al., 1999, 1997) or cold (Karashima et al., 2009; Nilius et al., 2012; Story et al., 2003) temperatures, voltage (Jensen et al., 2012; Voets et al., 2004), pH (Jordt et al., 2000; Tominaga et al., 1998), sodium (Jara-Oseguera et al., 2016), and ligands like capsaicin (Cao et al., 2013; Caterina et al., 1997; Gao et al., 2016) or the spider double-knot toxin (DkTx) (Bae et al., 2016; Cao et al., 2013; Gao et al., 2016). They are studied for their role in disease signaling (Nilius, 2007; Nilius et al., 2005), nociception (Story et al., 2003), as targets for drug delivery (Gunthhorpe and Szallasi, 2008; Nilius, 2013), and for their remarkable ability to sense temperature (Chugunov et al., 2016; Wen et al., 2016; Zheng and Qin, 2015). Indeed, the following TRP channels are responsible for temperature sensation and thermal regulation in humans: cold sensors TRPA1 ($T < 17$°C) and TRPM8 ($T < 25$°C), moderating sensor TRPV4 ($27 < T < 42$°C), and heat sensors TRPV3 ($T > 33$°C), TRPV1 ($T > 42$°C), and TRPV2 ($T > 52$°C) (Dhaka et al., 2006), where A, M, and V denote members of the ankyrin repeat, melastin-related, and vanilloid-binding TRP sub-families.

Recently, researchers have resolved the structure of TRPV1 in its open and closed configurations (Gao et al., 2016; Liao et al., 2013), which has led to a proliferation of research into the channel and its functionality (Bae et al., 2016; Cao et al., 2013; Jara-Oseguera et al., 2016; Jendryke et al., 2016; Zheng and Qin, 2015). The resolved TRPV1 structure is a homo-tetramer with its four monomers surrounding a central ion channel, as shown in Fig. 1(a) and (b). The monomers are further divided into the domains (Liao et al., 2013) shown in Fig. 1(c), i.e., the **C-terminal** (CT) domain, a relatively unstructured region which shares a role in thermosensation and ligand sensation (Brauchi et al., 2007; 2006; Raymond et al., 2014); the **TRP** domain, which mediates many interactions between the transmembrane and intracellular domains (Wen et al., 2016); the **transmembrane** domain, which resembles the transmembrane structure of voltage-sensing ion channels (Catterall, 2012, 2010); the extracellular **pore** domain, which controls dilation of the extracellular gate (Met644) (Grandl et al., 2010; Myers et al., 2008; Ryu et al., 2007) (a selectivity filter preventing anion passage); and the intracellular **linker** and **ankyrin repeat** domains, where the linker domain has been linked to thermosensation (Wen et al., 2016; Yao et al., 2011; Zheng and Qin, 2015) and the ankyrin repeats respond to myriad ligands (Gaudet, 2008).

The S6, S5, and pore helices create a channel between the intracellular and extracellular solutions which regulates ion passage and thus the ultimate sensation of an agonist. This ion channel is gated at both the intracellular and extracellular sides, with

* Corresponding author.
E-mail address: cmelni@umich.edu (C. Melnick).

https://doi.org/10.1016/j.jtbi.2018.02.004
0022-5193/

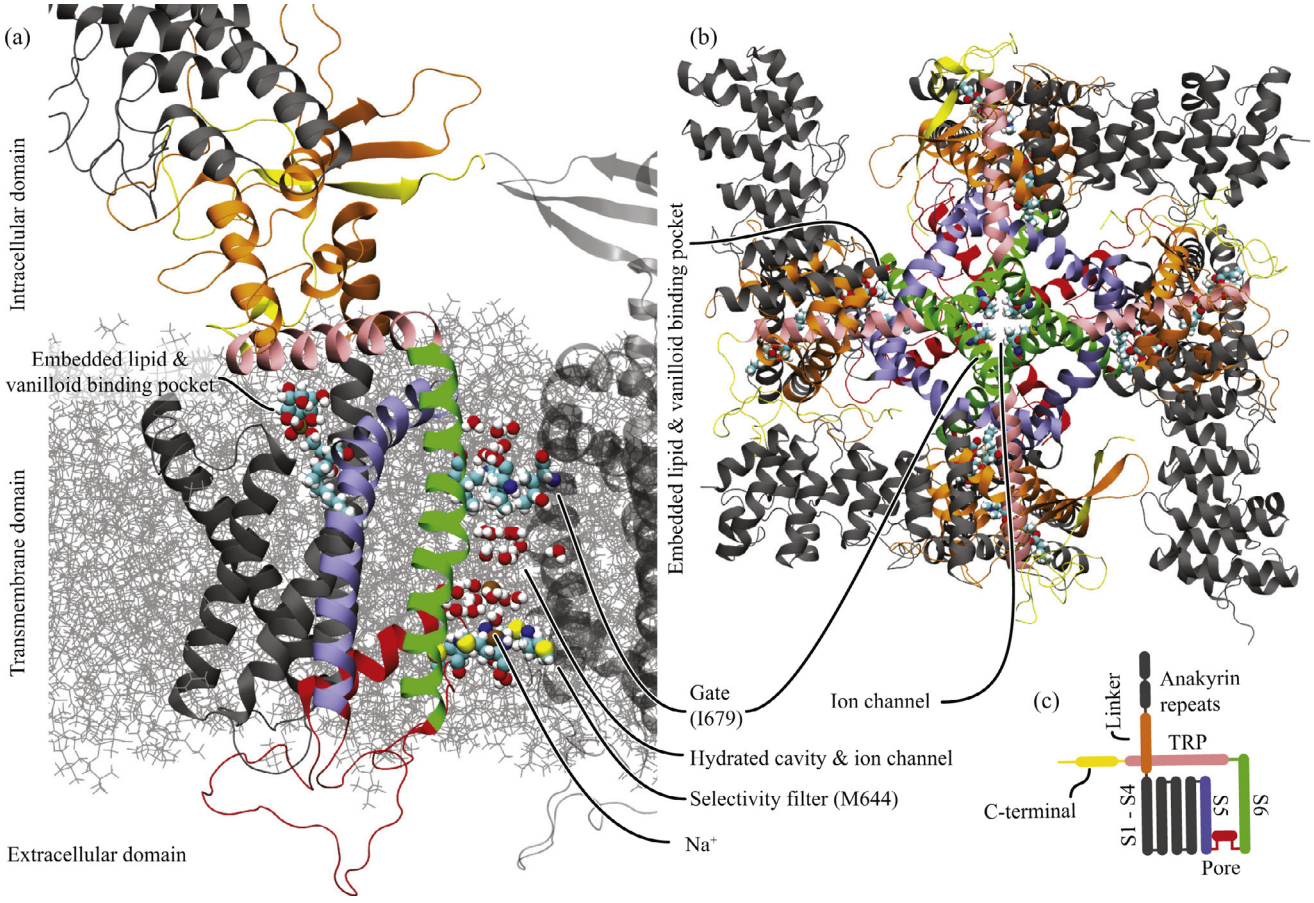

Fig. 1. The structure of TRPV1. (a),(c) One of four sub-units which comprise the rotationally symmetric assembly shown in (b). Together, these units form a thermally activated ion channel with two gates, Ile679 on the intracellular side and Met644 on the extracellular side. Between these gates resides a hydrated central cavity. Met644 primarily serves as a selectivity filter which excludes anions, while Ile679 forms a hydrophobic seal in the closed TRPV1 configuration shown here. Experimentally, lipids have been found to be embedded in the vanilloid binding pockets, and it is hypothesized that heat ejects them. Heat is also known to affect the pore, C-terminal, and linker domains. TRPV1 is shown here (Video 1).

a hydrated (Chugunov et al., 2016; Kasimova et al., 2017; Wen et al., 2016), central cavity between the two gates. The intracellular gate is formed by the four Ile679 residues on the S6 helix while the extracellular gate is formed by multiple residues near the pore helix (643—646; GMGD) (Liao et al., 2013). It is thought that the extracellular gate acts primarily as a selectivity filter, allowing the passage of cations but preventing the passage of anions (Liao et al., 2013); while the intracellular gate acts as a hydrophobic barrier which separates the intracellular and extracellular solutions (Chugunov et al., 2016), preventing ion passage unless it is opened.

The first structural study revealed two allosterically coupled actuation pathways which open these gates: one on the intracellular side and one on the extracellular side (Liao et al., 2013). Indeed, while the closed TRPV1 structure was resolved by cryo-EM imaging a TRPV1 channel with no ligands, the open TRPV1 required two ligands: one (double knot toxin, DkTx) bound to the extracellular pore domain, and one (resiniferatoxin, RTX) bound in the intracellular vanilloid binding pocket. Individually, these ligands dilated the extracellular selectivity filter and intracellular gate, respectively, but they did not open both gates. However, when both ligands were incorporated into the solution, both gates opened wider than they did when a single ligand was present (Cao et al., 2013; Liao et al., 2013).

In addition to structural studies, researchers have used mutagenesis studies to explore the function of the ion channel. These studies have uncovered many residues involved in the sensation of heat, most of which reside in the pore domain (Grandl et al., 2010; Myers et al., 2008; Ryu et al., 2007; Yang et al., 2010a, 2010b; Yao et al., 2010) and some of which reside in the CT domain (Brauchi et al., 2007, 2006) and around the vanilloid binding pocket (Hu et al., 2009; Yang et al., 2015). Because the vanilloid binding pocket and pore contain residues that affect both the thermal and also the vanilloid/DkTx sensitivity of TRPV1, researchers hypothesize that these vanilloids/DkTx activate TRPV1 through the same pathways that heat does. Thus, molecular dynamics (MD) studies have been performed on the TRPV1-DkTx (Bae et al., 2016) and TRPV1-RTX (Cao et al., 2013) complexes in an attempt not only to explain the ligand sensation pathways but also to explore the thermal activation pathways.

Researchers have also simulated the channel at various temperatures in order to directly explore the thermal activation pathways (Chugunov et al., 2016; Kasimova et al., 2017; Wen et al., 2016; Wen and Zheng, 2018). In combination, the structural, mutagenesis, and MD studies support the following hypotheses: (i) Increasing the temperature destabilizes the hydrophobic cluster in the pore and this ultimately leads to dilation and hydration of the extracellular selectivity filter; and (ii) a number of residues surrounding the vanilloid binding pocket respond to heat. However, the mechanism driving the latter response remains relatively unclear, and the role of the CT remains almost completely unexplored. For example, a few simulations suggest that the linker domain plays a crucial role in the intracellular activation pathway (Wen et al., 2016; Wen and Zheng, 2018; Zheng and Qin, 2015), undergoing a sub-

stantial enthalpy change upon heating due to the rearrangement of the hydrogen bonding network. Another recent simulation supports that the CT is, indeed, thermally activated (Raymond et al., 2014), but the connection of this domain to the activation pathway was not addressed. Furthermore, the most recent cryo-EM study of TRPV1 in a lipid nanodisk (Gao et al., 2016) shows that phosphatidylinositol lipids are embedded in the cold vanilloid pocket and that these lipids are displaced by RTX and other vanilloid agonists. Thus, the study hypothesizes that heat ejects these lipids much like the vanilloids do; however, there have been no simulations which attempt to support this hypothesis. Connecting and supporting the various hypotheses and creating a comprehensive hypothesis for the intracellular actuation pathway remains an important and major challenge in understanding the thermal actuation of TRPV1.

Here we present the first all-atom molecular dynamics simulations of the most recently reported structure, as shown in Fig. 1 and Video 1, so that we can address this challenge. Additionally, we incorporate the embedded lipids in order to test the recent hypothesis surrounding their role in thermal actuation. In the following sections, we discuss our methodology, present results replicating the current understanding of the extracellular actuation in the pore domain, explore the CT and linker domains and discuss their connection to the actuation of the vanilloid binding pocket, and investigate the role of the embedded lipids. While the complete thermal actuation of TRPV1 remains elusive, a number of structural changes are recorded which support our hypotheses and connect strongly to those discussed in the literature. Finally, mutagenesis experiments are suggested to test the proposed connection between the response of the CT and linker domains with that of the vanilloid binding pocket and displacement of the lipids embedded within them.

2. Molecular dynamics simulations, analysis methodology, and overarching results

This study is based on the all-atom MD simulation of TRPV1. A few methods of quantitative analysis are employed to digest the data produced from those simulations. In particular, we employ principal component, RMSD/RMSF, hydration, hydrogen bonding, and thermodynamic analyses. In the following sections, we discuss the details of these analyses and present results quantifying the response of the entire protein channel to heat.

2.1. Molecular dynamics simulations

This study uses the MD simulation code nanoscale MD (NAMD) (Phillips et al., 2005) with CHARMM36 (Huang and MacKerell, 2013; Klauda et al., 2010) force fields to simulate TRPV1. We use the most recent TRPV1 structure in the closed configuration (PDB accession number 5IRZ) (Gao et al., 2016) from the orientations of proteins in membranes (OPM) (Lomize et al., 2006) database for the C-terminal to linker domains. To this structure, we add the ankyrin repeat domain resolved and published in the previous TRPV1 structure (PDB accession number 3J5P) (Liao et al., 2013). The structure is protonated using PROPKA (Dolinsky et al., 2004), hydrated using DOWSER (Zhang and Hermans, 1996), and the missing pore loop is added and refined using the Rosetta loop modeling procedure (Kaufmann et al., 2010). The embedded lipids are taken from the 5IRZ structure. (In particular, we take the lipids with designations 6ES and 6O8.) Then, the protein and embedded lipids are embedded in a 170 × 170 Å POPC lipid bilayer membrane. We build this membrane using the visual molecular dynamics (VMD) (Humphrey et al., 1996) membrane builder and align it with the TRPV1 according to the specifications of the OPM database (Lomize et al., 2006). Any POPC lipids within 2 Å of the protein or embedded lipids are removed (619 remain). Finally, it is surrounded by the solvent: water with a 150 mM concentration of NaCl. We leave 25 Å of space between the periodic images of TRPV1, which requires 87,782 water molecules and a box of 170 × 170 × 150 Å.

Table 1
Molecular dynamics simulations.

Name	Temperature (K)	Elapsed time (ns)
HA	350	1250
CA	290	300
HB	350	1000
CB	290	500

We model the water using the TIP3P model (Jorgensen et al., 1983). All hydrogen bonds kept rigid in order to enables a 2 fs timestep. The nonbonded forces (van der Waals and electrostatics) are evaluated within a cutoff distance of 12 Å. The electrostatic problem is solved using the particle mesh ewald (PME) algorithm (Darden et al., 1993) every ten steps in order to update the long-range electrostatic forces. Temperature and pressure control are achieved using a Langevin thermostat with a friction coefficient of 2 ps^{-1} and a Nosé-Hoover Langevin piston at 1 atm (Feller et al., 1995; Martyna et al., 1994).

Two replicas of this structure are created by using the following relaxation procedure with different initial velocities and positions. A brief minimization is carried out in order to remove steric collisions. Then, we relax the lipid bilayer and solvent systems by restraining the embedded lipids and protein and during a 25 ns simulation of the system at 290 K. We restrain the protein and embedded lipids by applying a harmonic force based on the difference between the current and initial atomic positions. We then relax the entire system over an additional 125 ns, slowly reducing the harmonic force constants from the initial value of 0.5 to 0.001 kcal/(mol-$Å^2$). Following relaxation, the x and y dimensions of the box are fixed and the z dimension is allowed to fluctuate.

The resulting positions are used as a starting point for the production runs at 290 and 350 K. During production runs, the atomic positions (frames) are recorded every 10 ps for further analysis. The elapsed simulation times and the temperatures of runs conducted using these replicas are presented in Table 1. Note that we do not have production simulations of the experimentally resolved open configuration (5IRX). Instead, we focus our computational resources on the changes which occur to the closed configuration and avoid the issues surrounding the open structure (i.e., that it is resolved by using ligands and thus may differ from the heat activated open configuration). As simulating even 100 ns of this approximately 350,000 atom system requires massive computational effort, this focus is necessary to create relatively long trajectories. Indeed, while we would prefer to create additional replicas; simulate TRPV1 on the μs scale, simulate TRPV1 at additional, moderate temperatures, and include long, replicated simulations of the open configuration, doing so is not feasible at this time.

With the MD methodology established, let us quantify the stability of our simulations following relaxation and also examine the flexibility of the resulting, relaxed structure using root-mean-square displacement (RMSD) and fluctuation (RMSF) analyses. Here we calculate the RMSD and RMSF for each monomer using only the backbone C_α atoms. To do so, the C_α atoms of an individual monomer is fit to their initial, experimental positions (by minimizing the RMSD between them). The RMSF values are averaged in time for each residue (C_α atom) and across the monomers in order to quantify the flexibility of each residue, while the RMSD values are calculated for the entire monomer and then averaged across the four monomers in order to quantify the divergence of

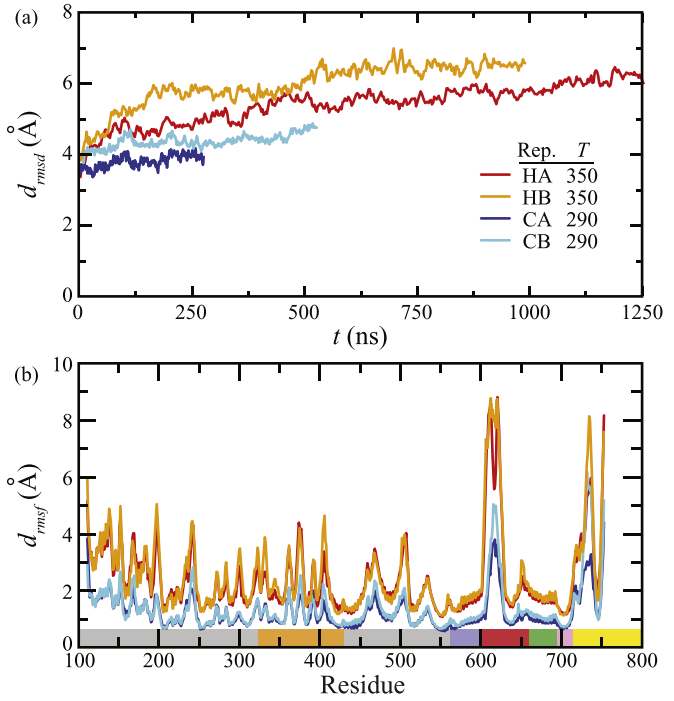

Fig. 2. (a) RMSD between the simulations and the initial, experimental structure (solid lines) over time and (b) RMSF of the TRPV1 monomers throughout the protein. TRPV1 is particularly flexible within the long pore loop which is missing from the experimental structure and the unstructured CT domain which was only recently resolved. The stable residues within the CT form a β-sheet with the Linker domain.

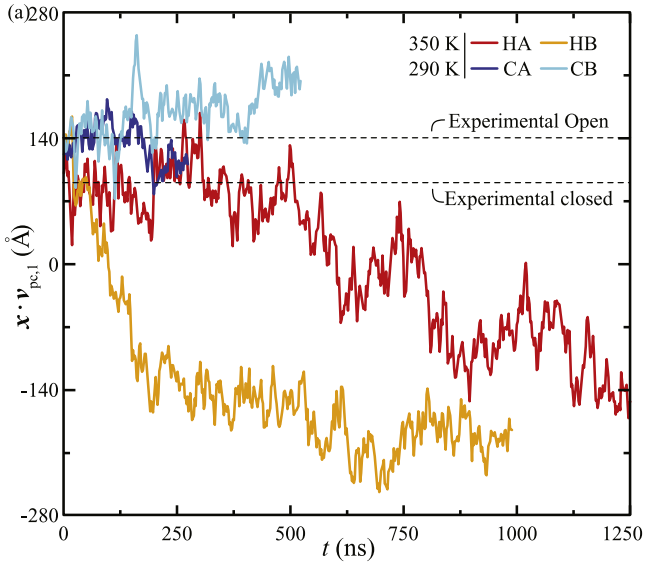

Fig. 3. Progress of simulations along primary component separating open and closed TRPV1. The eigenvector $\boldsymbol{v}_{pc,1}$ is normalized such that the open and closed experimental structures take values of ± 1. TRPV1 does not open in these simulations, although it does respond to heat.

the simulations from their initial states over time. The results are presented in Fig. 2.

As shown, the simulated TRPV1 structure differs notably from the experimental structure following the relaxation procedure. For example, the charged Sulfur group on residue Met644, which contributes to the selectivity filter at the extracellular pore of the ion channel, rotates out of the channel. Following this change, water molecules gradually pass through the filter and into the central cavity of the ion channel, hydrating it but not the intracellular gate (Ile679), which forms a hydrophobic seal (Chugunov et al., 2016). Then, an ion enters the cavity and a second ion slots into the selectivity filter between Met644 and Gly643, re-sealing the selectivity filter, as shown in Fig. 1 and the Video 2. (This behavior is discussed in more detail in Section 2.3.)

Additionally, the large degree of flexibility in the ankyrin repeat domain (as a whole), the unstructured CT domain, and long pore loop contribute substantially to the large RMSD. The pore loop and CT, in particular, change substantially during and following relaxation. Indeed, the RMSF plot, Fig. 2(b), shows RMSF values in these domains which exceedis 8 Å at 350 K or 6 Å at 290 K. This large degree of flexibility and instability in the CT and long pore loop is expected, as it explains the difficulty of resolving the structures experimentally and as these structures lack secondary structures. Most importantly, we do not record RMSD values which continue to diverge, i.e., the protein structures we are simulating are stable. Next, we apply a principle component analysis to the simulations in order to examine the differences between the hot and cold simulations and in order to quantify the openess of the hot simulations.

2.2. Principal component analysis

A principal component analysis (PCA) computes the axes upon which the data varies the most and thereby reduces the relevant dimensions of the problem (Jolliffe, 2002). The PCA uses the covariance matrix, C, of an ensemble of C_α atomic positions, which is given by the 3×3 block matrices

$$C_{ii'} = \frac{1}{M} \sum_m (\boldsymbol{x}_{im} - \langle \boldsymbol{x}_i \rangle) \otimes (\boldsymbol{x}_{i'm} - \langle \boldsymbol{x}_{i'} \rangle), \quad (1)$$

where m is the index of the frame in the ensemble of M frames and $\langle \boldsymbol{x}_i \rangle$ is the average position of the C_α atom in residue i across the ensemble (Wen et al., 2016). The eigenvalues of this matrix give the variance of the data when projected along the corresponding eigenvector ($\boldsymbol{v}_{pc,\alpha}$). Thus, the eigenvector corresponding to the largest eigenvalue ($\boldsymbol{v}_{pc,1}$) provides a direction of motion which separates the data most notably.

Here we use the PCA to examine the openness of the hot simulations, the closedness of the cold simulations, the thermal actuation, and the similarity between replicas at the same temperature. In particular, we are interested in the principal component which captures the difference between the hot and the cold structure. To calculate this component, we apply the PCA to all frames of all replicas. In order to weight the hot and cold simulations equally, we normalize the variance in the cold (hot) frames by the fraction of hot (cold) frames in the full ensemble. Then we compute the covariance matrix of this normalized ensemble of frames and calculate eigenvectors. Finally, we project the simulations upon the principal eigenvector ($\boldsymbol{x}_m \cdot \boldsymbol{v}_{pc,1}$). That is, we calculate the principal component. We also project the closed and open, experimentally resolved structures onto $\boldsymbol{v}_{pc,1}$ in order to examine the similarity of these structures to our simulations.

The results are shown in Fig. 3. As expected, $\boldsymbol{v}_{pc,1}$ separates the hot and cold replicas. Moreover, simulations at the same temperature behave the same when projected upon $\boldsymbol{v}_{pc,1}$. Thus, the principal component indicates a consistent response to temperature. Moreover, the open and closed experimental structures are separated in a qualitatively similar manner to the hot and cold structures, indicating that heat leads towards opening while the cold simulations remain quite similar to the initial closed structure. However, the hot simulations differ notably from the open, experimental structure when projected upon $\boldsymbol{v}_{pc,1}$.

The differences between the heated simulations and the open, experimental structure may arise for a number of reasons. These

include the computationally limited simulation time, issues with the experimentally closed structure, or the manner with which the open structure is resolved. That is, trajectories which extend well into the μs domain may be required to open TRPV1. Alternatively, a very recent MD study suggests that non-polar cavities in the extracellular side must by hydrated for thermally induced opening to occur (Kasimova et al., 2017), but DOWSER does not find these cavities. Thus, they are not hydrated in our structure and this could be preventing the complete, thermal actuation of TRPV1. Additionally, there are regions of the structure which are not completely resolved. The long pore loop is missing, for example, and it is modeled here using a Rosetta protocol that cannot consistently predict the structure of such a long loop. Additionally, the Ankyrin repeat domain is truncated in order to limit the computational demand, and the C-terminal domain is also truncated (as the final 100 residues have not been experimentally resolved). While neither the ankyrin repeat domain nor the final 100 residues of the C-terminal are expected to contribute to thermal sensation, the pore loop is expected to be central to it (Cao et al., 2013; Gao et al., 2016; Liao et al., 2013). Finally, the open structure is experimentally resolved using toxins rather than heat, which may lead to some structural difference. For any of these reasons, or a combination of them, our simulations do not capture the elusive opening of TRPV1 or show that the experimentally open structure is reached during the hot simulations. This is a common problem in MD simulations of thermal actuation in TRPV1 (Chugunov et al., 2016; Zheng and Qin, 2015).

2.3. Hydration and ion occupancy analyses

It has been proposed that hydration of the ion channel in TRPV1 controls its permeability and that the intracellular gate forms a hydrophobic seal (Chugunov et al., 2016). Thus, in addition to tracking the progress of TRPV1 along the primary components, we quantify the hydration of the ion channel. To do this, we align each snapshot of the protein and its nearby water molecules with the initial protein positions. Then we count the number of water molecules (oxygen atoms) within the ion channel as a function of the distance along the channel, z, and simulation time, t. Here the ion channel is defined as the central core of the simulation, i.e., $r < 5.5$ Å, where r is the radius from the center of TRPV1 on the $x-y$ plane. The resulting number distribution, $N_{H_2O}(z,t)$, is normalized into an occupation function, $f_{H_2O}(z,t)$, as follows. First, the simulation is divided into spatial (horizontal slices of the ion channel with thickness Δz) and temporal bins. Then we calculate the total number of water molecules found within each bin and divide by the total number of frames within each temporal bin to get a raw occupancy value. Here, we use 200 frames per bin ($\Delta t = 1$ ns) and spatial bins of height 0.35 Å. Due to the fluctuation of water molecules within the cavity and the small spatial bin size, it can be difficult to visualize the resulting occupation function. Thus, we renormalize this raw occupation function in order to examine the occupations between 0 and 0.25. That is, multiply our raw occupation function by four and set any value greater than one to one. The ion occupancy is calculated in the same manner, only we renormalize to the range between 0 and 0.1. Again, this renormalization is performed in order to produce illustrative figures.

The results are shown in Fig. 4. Three distinct regions are immediately apparent, particularly for replica CA (Fig 4(a)): The intracellular gate, which forms a hydrophobic seal (Chugunov et al., 2016) that allows neither water nor ions into or through it; the cavity, which is typically filled with many water molecules and a single sodium cation; and the selectivity filter, which typically holds a single cation and is bracketed by two spaces inhabitted by water molecules. No anion is found in the channel at any frame. We call these the typical conditions in our following discussion.

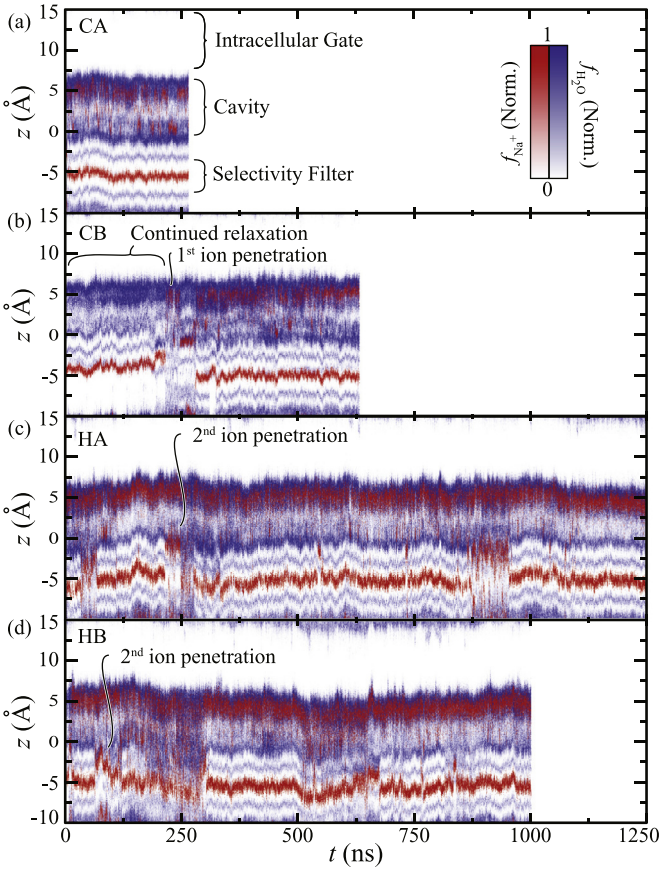

Fig. 4. Hydration of and ion incursion into the central ion channel of TRPV1 in the cold replicas (a) CA and (b) CB and hot replicas (c) HA and (d) HB. After relaxation, the intracellular gate forms a hydrophobic seal, while the extracellular selectivity filter forms a hydrophobic seal with the addition of a cation (Gly643 - cation - Met644). In hot simulations, this complex is occasionally perturbed, with the cation moving into the central channel. A water molecule tends to replace it and hydrate the filter. This is shown in Video 2.

While the intracellular gate remains closed in all of our simulations, notable deviations from this typical behavior arise. Let us discuss these differences.

First, let us examine the other cold replica, CB. In the first 200 ns of this simulation, there is no ion in the central cavity, and the selectivity filter does not have a water molecule immediately below it. Between 200 and 300 ns, the first ion enters the central cavity, additional water molecules follow it, and a new ion enters the selectivity filter. After 300 ns, the ion channel behaves in the typical manner. We believe that the initial phase describes the continued relaxation of this replica towards its ground state. During this relaxation (and the initial relaxation of replica A) the sulfur group on residue Met644 rotates away from the selectivity ion channel. This allows water to fill the now vacant space below the filter and potentially encourages or allows the first ion to enter the central cavity.

In contrast, the hot simulations show continued and consistent deviation from the typical behavior. Primarily, we see that the ion lodged in the selectivity filter occasionally escapes, briefly enters the central cavity (2nd ion penetration), and then returns to the selectivity filter. When the ion leaves the selectivity filter, water molecules can fill the selectivity filter. Indeed, a contiguously hydrated path forms from the extracellular solution to the intracellular gate, as shown in Video 2. This contrasts with the filter-ion complex which does not allow water to pass between the extracellular solution and central cavity. Thus, we consider the selec-

tivity filter without (with) a cation lodged between Gly643 and Met644 to be open (closed). With this perspective, the selectivity filter is seen to flicker between the open and closed states at 350 K but remains closed at 290 K. This flickering of the selectivity filter from the closed to open state has been observed experimentally (Cao et al., 2013; Hui et al., 2003) and within other simulations (Wen et al., 2016) at high temperatures. Before we investigate the local structures in TRPV1 which explain its thermal sensitivity, let us first examine the overall hydrogen bonding picture and the thermodynamic behavior of TRPV1 when subjected to heat.

2.4. Hydrogen bonding and thermodynamic analyses

Examining changes in the hydrogen bonding network should indicate which domains and residues are important in thermal sensation. Indeed, hydrogen bonding networks have been proposed as a crucial component in the response of molecules, supramolecules (Ware et al., 2012) and liquid crystals (Jiang et al., 2013) to temperature changes. Consider that the temperature sensation in TRPV1 (and the cold sensor TRPM8) can be explained thermodynamically by the large increase (decrease) in energy and entropy as the molecule shifts from its open to closed configuration (Clapham and Miller, 2011; Voets et al., 2004), and consider that breaking a hydrogen bond will tend to increase both thermodynamic quantities. Therefore, the rearrangement of the hydrogen bonding networks in TRPV1 is expected to be central to its ability to sense temperature (Zheng and Qin, 2015). However, hydrogen bonding is not the sole contributor to the thermal sensitivity of proteins. Indeed, the enthalpy of a protein primarily changes through the exposure of hydrophobic residues to the solution (Clapham and Miller, 2011). While we focus on hydrogen bonding as indicators of the local mechanisms through which thermal actuation is accomplished, the hydrophobic surfaces exposed during actuation largely enable this actuation to occur from a thermodynamic perspective. Let us first evaluate the overall hydrogen bonding picture in order to determine on which regions of the TRPV1 we should focus our analysis.

Here we compare the occupation of the hydrogen bonds in the cold and hot simulations in order to discover the bonds and regions which are most crucial to thermal sensation in TRPV1. A hydrogen bond (HB) is quantified as a pair of polar atoms within 4 Å of each other and with a donor-hydrogen-acceptor angle deviating from a straight line by less than 60°, and the VMD (Humphrey et al., 1996) program is used to find these HB's in all of our simulations. From this data, we calculate the average HB occupation between two residues i and j ($f_{\mathrm{HB},ij}$) and the difference in the average HB occupation between the hot and cold trajectories ($\Delta f_{\mathrm{HB},ij}$). Here all replicas are considered, and the first 250 ns of the hot trajectories is discarded to capture the difference between the hot and cold trajectories more accurately. (That is, we discard the "cold" portion of the hot trajectories. In general, $\Delta f_{\mathrm{HB},ij}$ grows as we discard more of the hot trajectory.) We note that if a pair of residues form multiple hydrogen bonds, the occupation of these bonds are summed together. We also calculate confidence intervals for $f_{\mathrm{HB},ij}$ and the standard deviation in the hydrogen bonding occupation groups of 50 frames, the results of which are presented in the supplementary materials for selected hydrogen bonds. The total occupation of each hydrogen bond in the cold and hot simulations are also shown in Fig. S1. Finally, the supplementary materials presents the distance between residue pairs which form notable hydrogen bonds and the correlation in the distance between selected residue pairs. Despite these analyses, some caution must be applied to the hydrogen bonding analyses: We have not conducted simulations at additional, more moderate temperatures. Thus, meta-stable hydrogen bonds may remain in the 290 K simulations which would break at 310 K. Conversely, stable hydrogen bonds may break in the 350 K simulations which would not break at 335 K. If it were not for our computational limits, we would conduct simulations at additional temperatures in order to validate our analysis. Instead, we use the literature to support our analysis and note where no such support exists. Moreover, we try not to integrate unsupported mechanisms into our final hypothesis.

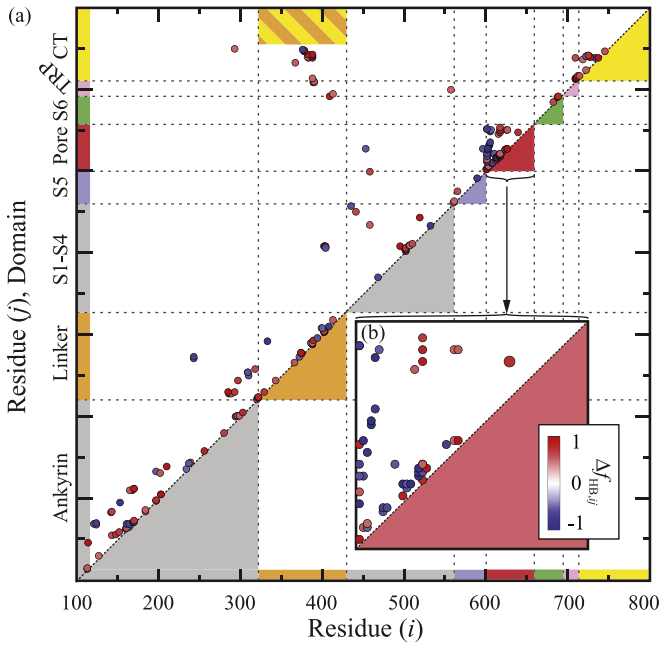

Fig. 5. (a) The difference in hydrogen bonding occupation (Δf_{HB}) throughout TRPV1 and (b) in the pore domain after heating, from a combined data set of all replicas. Figs. 7(b) and 8(b) zoom in on other important domains. Only hydrogen bonds with an occupation difference exceeding 0.5 are shown. A substantial number of hydrogen bonds are broken in the pore domain, supporting its role in thermal actuation. Additionally, a number of bonds form and break within and between the CT and linker domains. Finally, there are few major cross-domain bonds within the vanilloid binding pocket which respond to heat.

A number of hydrogen bonds form and break after subjecting TRPV1 to the 60 K change in temperature, as shown in Fig. 5. The highest concentration of these changes occur in the pore, where a substantial number of hydrogen bonds break. The second highest concentration of these changes occur in the region where the linker and CT domains are enmeshed (CTL domain). Finally, the hydrogen bonding network surrounding the embedded lipids in the vanilloid binding pocket (VBP) changes substantially upon heating. These three areas will remain the focus of our investigation as we proceed. Before delving into the hydrogen bonding networks within these domains, let us examine the overall thermodynamics of TRPV1, particularly in the pore and CTL domains where hydrophobic residues may be exposed to the solution.

The potential energy of TRPV1 and its subdomains are evaluated in the following manner. For a given frame, we calculate the internal energy (all bond and non-bonded energy contributions) of a selection (e.g., a single monomer or a subdomain within that monomer) and the energy between that selection and the surrounding solution, lipids, and protein systems using NAMD. Then we find the total energy by summing across these four contributions. For a single time, we average the results across the nearest 50 frames. In this manner, we sample the potential energy of a given selection in time steps of 125 ns. The overall energy of a selection is then found by averaging across the monomers and all cold and all $t > 250$ ns hot data points. The entropy is calculated using the MD analysis code carma Glykos (2006) using the Schlit-

Table 2
The potential energy due to interactions with the solution (U_{H_2O}), the total potential energy (U), and the entropy (S) of a TRPV1 monomer, its pore, CT, and CTL domain ± the standard deviation.

Domain	U_{H_2O} (meV)	U (meV)	S (meV/K)
TRPV1 (350 K)	-612.1 ± 24.4	-686.2 ± 12.6	104.7 ± 1.8
TRPV1 (290 K)	-695.0 ± 14.1	-804.3 ± 8.5	91.8 ± 2.2
TRPV1 (Δ)	82.9 ± 38.5	118.1 ± 21.08	12.9 ± 4.0
Pore (350 K)	-66.2 ± 8.7	-73.1 ± 7.2	31.6 ± 2.1
Pore (290 K)	-86.4 ± 9.3	-86.4 ± 3.1	25.2 ± 1.5
Pore (Δ)	20.2 ± 18.0	13.3 ± 10.27	6.4 ± 3.7
CT (350 K)	-183.3 ± 10.3	-256.5 ± 6.0	-
CT (290 K)	-207.6 ± 10.3	-280.7 ± 5.3	-
CT (Δ)	13.1 ± 15.7	7.1 ± 8.4	-
CTL (350 K)	-183.3 ± 10.3	-256.5 ± 6.0	62.1 ± 1.9
CTL (290 K)	-207.6 ± 10.3	-280.7 ± 5.3	53.7 ± 2.0
CTL (Δ)	24.3 ± 20.6	24.3 ± 11.3	8.4 ± 3.9

ter method (Schlitter, 1993), i.e., by quantifying the variation of a selection across an ensemble of frames using a PCA. Here we restrict our analysis to the C_α atoms of a given selection, which gives more consistent results and helps to avoid the creation of negative eigenvalues of the PCA matrix. We perform this analysis on ensembles of 500 frames spanning 250 ns with a starting time incremented by 125 ns. The overall entropy of a selection is then found by averaging the entropy across the monomers and all cold and the $t > 250$ ns hot frames. The results are presented in Table 2 for the entire protein, the pore domain, CT domain, and the combined CT and Linker (CTL) domains. Note that the ankyrin repeat domain is not included in the TRPV1 evaluation, as the harmonic approximation does not appear to be reasonable within this domain. That is, a large number of negative eigenvalues are generated, and the Schlitter method predicts unreliable or undefined entropy values.

As shown, both entropy and energy increase in TRPV1 after it is subjected to heat. Moreover, much of the energy change is due to the interactions between the pore and CTL domains with the solvent, i.e., due to the exposure of hydrophobic residues to water. These trends fit well with the current understanding of TRPV1 and other heat (or cold) sensors. That is, the free energy change between the closed and open configurations becomes negative only when the temperature rises (or drops) below a threshold value. Thus, this thermodynamics analysis supports the role of the CTL and pore domains in driving the thermal actuation of TRPV1. Moreover, the protein-solution interactions dominate the energy change, indicating that hydrophobic exposure drives their thermal response. However, the enthalpy and entropy of a given configuration are not generally independent of the temperature (Clapham and Miller, 2011), which prevents us from using these parameters to model the thermal activation curve of TRPV1 as in Ref. Voets et al. (2004). In the remainder of this study, we do not focus on this sort of thermodynamic quantification. However, we do note that the total energy change is comparable with the enthalpy changes used successfully in such modeling efforts. Instead, we focus on the mechanisms through which the initial exposure of hydrophobic residues leads towards the ultimate opening of the TRPV1 ion channel.

3. Results and discussion

First, let us examine the most well-studied structure that is responsible for the thermal actuation of TRPV1: the hydrophobic clusters in the extracellular pore domain. Then we will focus on the rearrangement of the CT and linker domains. Finally, we will investigate the vanilloid binding pocket and discuss the role of the embedded lipids.

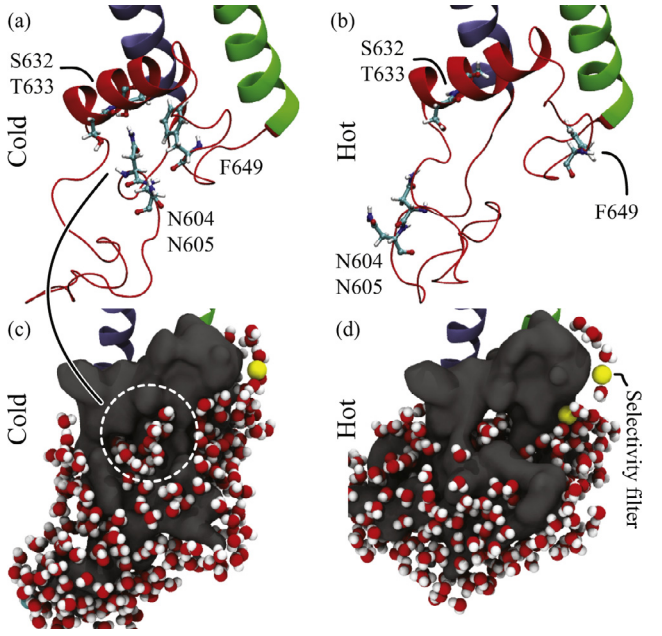

Fig. 6. The pore domain in (a,c) cold and (b,d) hot TRPV1. A hydrophobic cluster in the pore domain dissolves after heating from 290 to 350 K, shown by (a,b) the rotation of the long (Asn605, Asn604) and short (Phe649) pore loops away from the pore helix (Ser632,Thr633), and (c,d) the incursion of water into the pore structure. This hydrophobic destabilization frees the selectivity filter to occasionally flicker into the open, hydrated state, as shown in Fig 2(b). This pore transition is shown in Video 3.

3.1. Hydrophobic destabilization in the extracellular pore

The pore structure contains a short helix and two loops which connect the pore helix to the S5 and S6 helices. The prominent theory regarding its thermal actuation is as follows: a number a hydrophobic residues in these loops form a hydrophobic cluster that is stable at low temperatures but disassociates at high temperatures. This disassociation allows water to infiltrate between the pore loops, which reorganize in response, reducing the stiffness of the selectivity filter and encouraging the flickering of the filter into an open state (Bae et al., 2016; Chugunov et al., 2016; Wen et al., 2016). Our results, presented below, support this hypothesis.

In addition to finding that the enthalpy of the pore increases drastically due to the pore-solvent interactions (Table 2), we find that a large number of hydrogen bonds break within the pore domain, as shown in Fig. 5. In particular, we find a cluster of crucial hydrogen bonds between residues Ser632 and Thr633 on the pore helix, residues Asn604 and Asn605 on the S5-side loop, and Phe649 on the on the S6-side loop. These bonds break upon heating, allowing the pore loops to unfold, as shown in Fig. 6(a) and (b) and in the Video 3. The behavior of these hydrogen bonds is shown quantitatively in the supplemental materials Figs. S2 (time-domain) and S10 (correlations). Of these residues, mutagenesis experiments (Grandl et al., 2010; Myers et al., 2008; Ryu et al., 2007) and molecular dynamics (Chugunov et al., 2016) simulations have highlighted the importance of Thr633 and Phe649 in temperature sensation. We must note that these hydrogen bonds do include residues from the long pore loop (Asn604, Asn605), and that this loop is modeled within Rosetta. As Rosetta is cannot consistently predict such a long protein loop, we must question results which involve its thermal response. For example, the hydrogen bonds formed by this loop may simply be unstable and break more quickly in the hot trajectories than in the cold ones. However,

the thermally active hydrogen bonds involving these loops occasionally and briefly break and then reform in the cold simulations. Thus, they appear to be stable within the structure predicted by Rosetta.

Following the destabilization of the hydrophobic cluster, water penetrates into the structure as shown in Fig. 6(c) and (d). The pore loops simultaneously reorganize, as quantified by the addition of a few hydrogen bonds within the long pore-loop (Glu600 - Lys603 and Asn628 - Ser626). Mutagenesis experiments support these observations, as altering residues at Glu600, Lys603, and Asn628 reduce the thermal sensitivity of TRPV1 (Grandl et al., 2010; Myers et al., 2008; Ryu et al., 2007).

These changes increase the permeability of the extracellular selectivity filter and should allosterically encourage the dilation of the distal intracellular gate. However, we record a negligible number of frames depicting TRPV1 with an open intracellular gate. Thus, we can only suggest the following, weakly supported hypothesis. We find two thermally responsive hydrogen bond connecting the pore domain and the S5 helix: Asn628 - Val596 and Thr641 - Tyr584. Noting that residue Thr641 have been identified in previous simulations as coupling the pore and S6 helices (Wen et al., 2016), and as Asn628 has been identified in mutagenesis experiments, we hypothesize that the allosteric coupling is mediated through these residues. Indeed, following the hydrophobic destabilization, Thr641 moves away from Lys584 and repositions along the S6 helix, which should encourage the dilation of the intracellular gate. However, the correlation of these hydrogen bonds with the temperature and the other hydrogen bonding changes in the pore are weak, as shown in Figs. S2, S3 and S10, and the supplementary Table S1.

3.2. Intracellular rearrangement surrounding the C-terminal

Substantially less is known about the intracellular than the extracellular mechanisms, particularly those in the CT domain. Raymond *et al.* were the first to simulate the CT, but they did so without a resolved experimental structure or a representative environment (Raymond et al., 2014) (e.g., the lipid membrane or neighboring linker domain). Similarly, the role of the linker domain has only recently been explored (Wen et al., 2016; Zheng and Qin, 2015). Here we present our findings on these domains in order to support or expand upon these studies.

Following heating, there is a substantial change to the hydrogen bonding network between the linker and CT domains, as shown in Figs. 5(a) and 7(b). Nearby, we also record consistent changes to the hydrogen bonding network between the first few residues in the CT and the last few residues on the TRP helix. However, creating a consistent description of the changing hydrogen bonds in the CT domain is challenging: As with the long pore loop, the CT lacks substantial secondary structure. Therefore, it has the freedom to move around substantially, even at 290 K, limiting deterministic observations. For example, Figs S4, S5, and S6 show the large variation in the distance the between important residue pairs discussed below.

Two secondary structures provide the majority of the CT stability: a β-sheet formed between the CT and linker domains (CT residues 741 to 750 and linker residues 368 to 383) and the TRP helix. The long CT loop between these structures holds the thermally responsive clusters. In particular, we find two distinct areas which react to heat: (CTL.i) The N-terminal of the CT domain (713–720), which forms various, short α-helices next to the TRP helix after heating (in some cases, it joins and extends the TRP helix, as shown in Fig. 7); (CTL.ii) the middle of the loop, which forms a cluster with itself under low temperatures (CT cluster) and (CTL.iii) with the linker domain under high temperatures (CT-linker, or CTL,

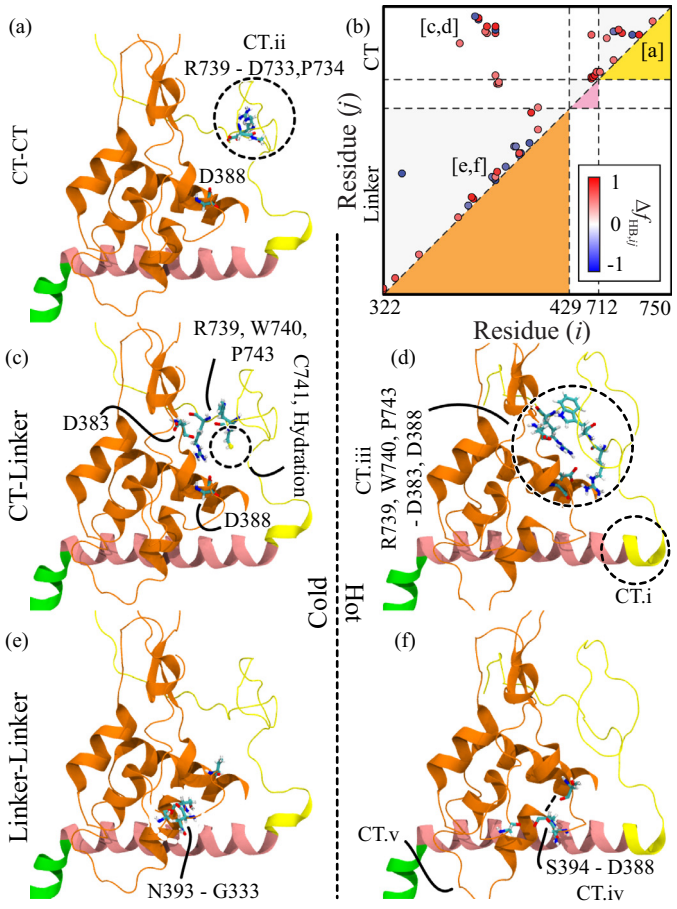

Fig. 7. Representative CT and linker structure before (a,c,e) and after (d,f) heating of TRPV1. (b) Hydrogen bonding changes in the CT-linker (CTL) complex. (a) The cold TRPV1 CT forms a cluster in the long loop between the TRP helix and linker-CT β-sheet, (c) with water penetrating between the two domains. After heating, the CT cluster dissolves and new cluster forms between CT and linker domains (d). There is further, weaker evidence that this new cluster pulls an important linker helix away from the vanilloid binding pocket due to a hydrogen bond between Asp388 - Ser394. The cluster transition is shown in Video 4.

cluster), as shown in Figs. 7(a), (c), and (d). A representative transition is also shown in the Video 4.

We hypothesize that (CTL.i) precedes and encourages (CTL.ii), by shortening the CT loop, displacing key residues in the cold CT cluster, and forming hydrogen bonds with the CT cluster. Additionally, (CTL.i) may directly influence the linker residues (CTL.iii) through hydrogen bonds. New hydrogen bonds are rare between CTL.i and the CT or CTL clusters, however, and do not correlate notably to the changes occurring throughout the CTL domain as shown in Figs. S4 and S5. Furthermore, no mutagenesis experiments nor molecular dynamics simulations have identified the CT residues in this region (713–720) as important to the thermal actuation of TRPV1. Thus, it is possible that the thermal response of this region does not affect the rest of the CT or the surrounding structures. In contrast, a key residue in the CT and CTL clusters, Ala739, was previously identified by Raymond et al. (2014), as well as other residues involved in the CT cluster, Trp740 and Cys741, and CTL cluster, Arg743 and Asp745. Furthermore, the thermal response and correlations are much more evident in the CT and CTL clusters than in the CT-TRP complex, as shown in Figs. S6, S11, and S12(a) and (b). Thus, we can more reasonably expect that (CTL.ii/CTL.iii) influences thermal actuation. Additional mutagenesis studies focused on the CTL domain are required to support the role of either mechanism, however.

There is little evidence for the mechanism through which this change influences the intracellular gate. However, the hydrogen bonding analysis provides a possible pathway: (CTL.ii) the CT cluster breaks and (CT.iii) the CTL cluster forms, re-positioning the short linker helix, 384 to 389; (CTL.iv) this pulls on the linker helix above the vanilloid binding pocket, 405 to 394, quantified by the increase in hydrogen bond Thr389 - Ser394 and decrease in hydrogen bond Asn393 - Gly333, as shown in Figs. S7 and S12(c); and (CTL.v) this in turn pulls on the linker loop above the vanilloid binding pocket.

From the literature, Zheng and Qin also found thermally responsive residues in these regions using limited simulations of the experimental open and closed structures (Zheng and Qin, 2015). In particular, they noted large enthalpy changes around the short helix central to (CTL.iii) and (CTL.iv) and the linker loop central to (CTL.v). In a later article (Wen et al., 2016), longer simulations did not reveal that hydrogen bonds involved in (CTL.ii-iv) were thermally active; however, these simulations did not involve the CT domain. This supports the crucial role of the CT domain in activating the linker domain. Indeed, the thermodynamic analysis shows that the interactions between the CT domain and the solvent dominate the enthalpy gain of the CTL region, as shown in Table 2. All other simulated and experimental evidence of linker domain involvement is limited to the vanilloid binding pocket. In the next section we discuss how (CTL.v) affects the vanilloid binding pocket and lead to the thermal actuation of TRPV1. In the conclusions, we will discuss experiments that could test the hypothesized mechanisms (CTL.ii-v).

3.3. Displacement of embedded lipids in the vanilloid binding pocket

The vanilloid binding pocket created by the S5-S4 linker, TRP helix, a linker domain loop, and the S1-S4 helices has been extensively investigated (Cao et al., 2013; Kasimova et al., 2017; Wen et al., 2016), as it was used to resolve the open structures of TRPV1 (Gao et al., 2016; Liao et al., 2013). While its thermal actuation is debated, a recent hypothesis posits that heat displaces lipids embedded in the vanilloid binding pocket (VBP), that a new hydrogen bond forms between the S5 helix and the S4-S5 linker (Arg557 - Glu570), and that this ultimately leads to the dilation of the intracellular gate (Gao et al., 2016).

In general, we support this hypothesis. Nearly all of the embedded lipids are displaced from the VBP when subjected heat. Furthermore, lipid displacement correlates strongly with the formation of the Arg557 - Glu570 HB, as shown in Figs. S9 and S13. However, while the Arg557 - Glu570 HB almost always and quickly forms after the lipid is displaced, the hydrogen bond can form without lipid displacement. Moreover, of the eight lipids embedded in the vanilloid binding pocket (two hot replicas with four monomers), only one was completely ejected from the VBP. This ejection occurs around 600 ns into the simulation, suggesting that this process is slow and further ejection will occur as the simulation domain extends into the microsecond range. Despite these caveats, the Arg557 - Glu570 HB is clearly encouraged by and correlated with the heat activated lipid displacement.

Before the lipid displacement occurs, the VBP tends to change. This is quantified here through the changes in the hydrogen bonding network, as shown in Figs. S9 and S13. (These changes also correlate with the formation of the Arg557 - Glu570 HB, as shown in Figs. S9 and S14.) Thus, we hypothesize that the structural rearrangements shown in Fig. 8(a) and (c) precede and encourage lipid ejection, the formation of the Arg557 - Glu570 HB, and the opening of the intracellular gate. Let us discuss the changes which occur after heating and (typically) before the lipid displacement. Three regions rearrange consistently upon heating: (VBP.i) the nearby linker loop, (VBP.ii) the S6 and TRP helices, and (VBP.iii) the loop linking the S3 and S2 helices, as shown in Figs. 8 (e,f), (d), and (g,h), respectively. We discuss these in order before describing the changes which follow lipid displacement.

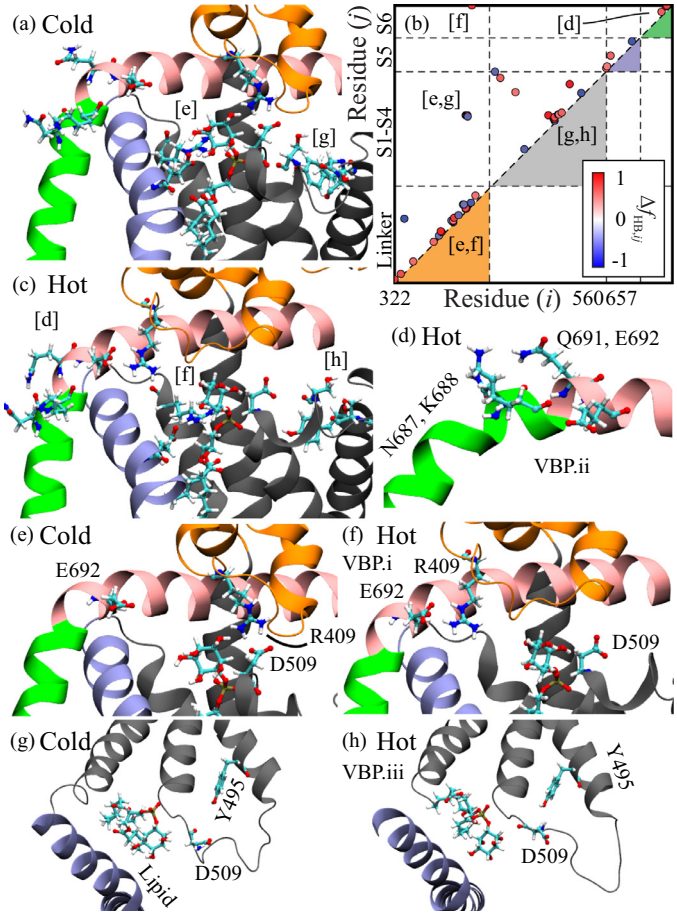

Fig. 8. (a,c) The vanilloid binding pocket and key residues within it, (d,e,f,g,h) the sub-regions within, and (b) the major hydrogen bonding shifts. Central to these changes is the loss of the Arg409 - Asp509 hydrogen bond and subsequent formation of the Arg409 - Glu692 and Asp509 - Tyr495 hydrogen bonds. In combination, these changes open up the vanilloid binding pocket, such that the embedded lipid is exposed to the environment and can be displaced or ejected. Additionally, we observe the TRP and and S6 helices hybridize after heating. This transition is shown in Video 5.

(VBP.i): In the cold TRPV1 replicas, residue Arg409 on the nearby linker loop forms hydrogen bonds with residue Asp509 in loop connecting the S2 and S3 helices. This bond breaks after heating, as shown in Figs. 8 (e) and (f) and S9. Then, Arg409 rotates to join a cluster of residues which forms in the linker loop (399 to 405) and/or forms hydrogen bonds with Glu692, as shown in Fig. S13. Both of these temperature dependent hydrogen bonds were noted in previous simulations of TRPV1 (Wen et al., 2016), but not in previous mutagenesis studies. Additionally, it has been noted that this linker loop experiences a substantial change in enthalpy as it shifts from the closed to open configurations (Zheng and Qin, 2015). Here we posit that the Arg409 - Asp509 hydrogen bond is the lock which ultimately restrains the embedded lipid, preventing its ejection. However, the lipid displacement can occur without the Arg409 - Asp509 HB breaking, as shown in Fig. S13(c). Furthermore, we suggest that this rearrangement is a result of the distal CT and linker domain rearrangement, as discussed in the previous section (CTL.v). However, correlations with distant hydrogen bonding changes are weak.

(VBP.ii): The most consistent hydrogen bonding change occurs between the S6 (Asn687, Lys688) and TRP helices (Gln691, Glu692), as shown in Fig. 8(b) and S8. These helices are distinct in cold TRPV1 but occasionally hybridize in hot TRPV1. That is, the C-terminal turn of the S6 helix and N-terminal turn of the TRP helix bend toward each other and form hydrogen bonds like those in a single α-helix. This change is shown in Fig. 8. This hybridization is connected to (VBP.i) through the Glu692 - Arg409 hydrogen bond. (VBP.i) tends to occur first, as shown in Figs. S9 and S8, and we hypothesize that it helps to stabilize (VBP.i) by re-positioning Glu692 nearer to Arg409. (VBP.i) can occur without the Arg409 - Glu692 hydrogen bond forming. Thus, (VBP.ii) may be relatively independent of the other changes occurring the VBP and CTL domains, and it may not affect dilation of intracellular gate. However, it is prominent in our simulations and next to the gate itself, and the Glu692 - Arg409 HB has been identified as a thermally active hydrogen bond which forms in the hot, open structure (Wen and Zheng, 2018). Thus, we hypothesize that it does play a role in the thermal actuation of TRPV1.

(VBP.iii) The loop between S2 and S3 helices changes substantially after heating. This change occurs after the Arg409 - Asp509 hydrogen bond breaks, which enables Asp509 and Tyr495 to form a new hydrogen bond. Additional rearrangement occurs as the residues around Ser505 and Ser502 form a cluster, with Ser505 - Ser502 forming a new hydrogen bond to stabilize it. These changes correlate strongly to both lipid displacement and the Glu570 - Arg557 HB, as shown in Fig. S13 and S14. Thus, we hypothesize that changes in this loop further expose the embedded lipid to the bilayer and intracellular solution, encouraging its ejection. However, the S1 to S4 helices are generally believed to be a static domain responsible for voltage sensation, and the Arg409 - Asp509 hydrogen bond represents the sole appearance of this loop in the literature (Wen et al., 2016).

To summarize, the Arg557 - Glu570 hydrogen bond also forms when RTX is embedded in the VBP of TRPV1 (Gao et al., 2016), and it was suggested that this hydrogen bond pulls the S4-S5 linker (which contains Glu570) away from the ion channel, leading to or encouraging the dilation of the intracellular gate. Thus, our results support their hypothesis that heat displaces the embedded lipid and this leads to gate dilation through a similar mechanism to the RTX agonist. We add to this hypothesis by suggesting that the distal CT - linker complex initiates lipid ejection by pulling on the proximal linker loop (CTL.v) and ultimately breaking the Arg409 - Asp509 hydrogen bond (VBP.i). However, our results do not indicate that the formation of the Arg557 - Glu570 hydrogen bond requires the ejection of the embedded lipid. As shown in Fig. 9(d), the bond can still form when the inositol ring of the lipid is displaced away from the elbow of the S4-S5 linker, but it is not completely ejected from the VBP. Still, this does not modify the hypotheses significantly: (VBP.i) Heat breaks the Arg409 - Asp509 hydrogen bond, (VBP.iii) leading to rearrangement around the vanilloid, and (VBP.iv) enabling the embedded lipid inositol ring to move slightly or completely out of the pocket. (VBP.v) Then the S4-S5 linker is pulled away from the central axis of TRPV1 by the Arg557 - Glu570 hydrogen bond, encouraging the dilation of the intracellular gate. The lipid ejection and vanilloid binding pocket transition are shown in Video 5, while the overall intracellular activation pathway hypothesis is illustrated in Fig. 10. Furthermore, statistical analysis of the hydrogen bonds discussed and other surrounding bonds are presented in Table 2.

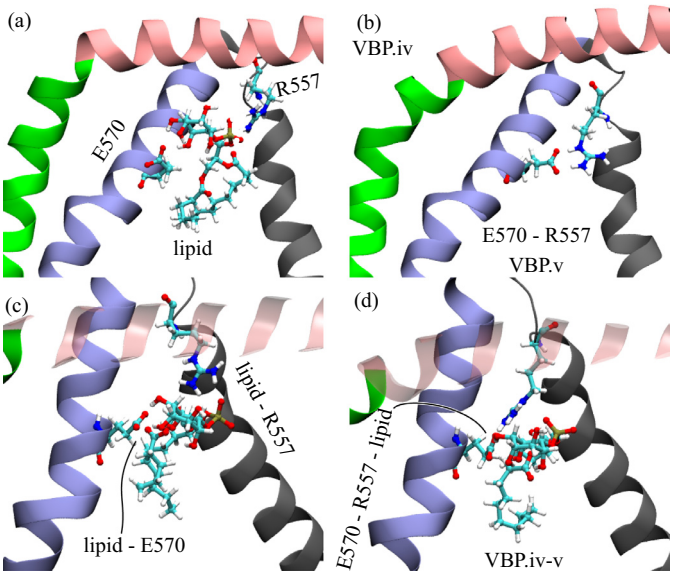

Fig. 9. (a,c) Cold and (b,d) hot snapshots of the embedded lipid. Before heating, the lipid forms hydrogen bonds with residues Glu570 and Arg557. After heating, the lipid is displaced (d) or ejected (b), allowing residues Arg557 and Glu570 form a hydrogen bond. This new bond pulls the S4-S5 linker away from the central axis and encourages dilation of the intracellular gate. The lipid ejection is shown in Video 5.

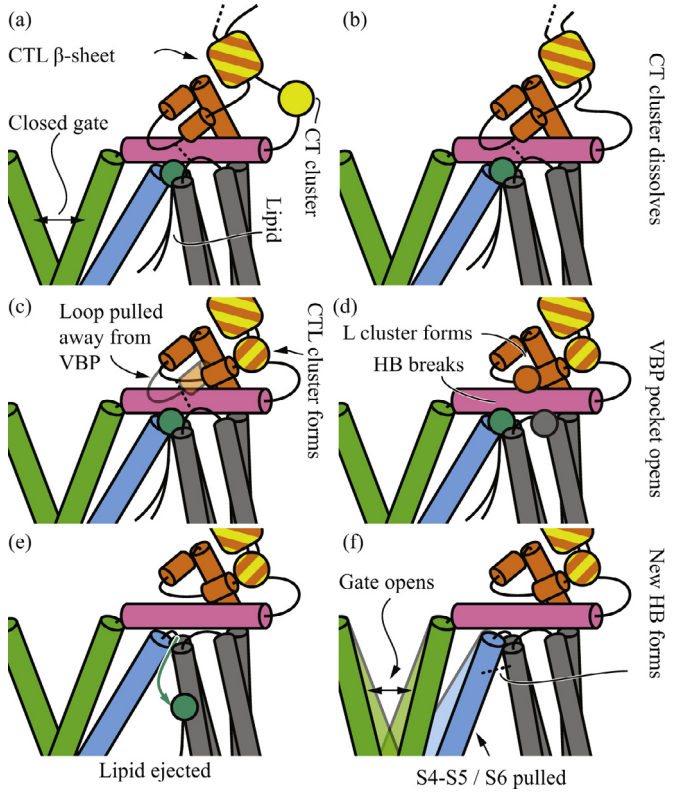

Fig. 10. Overview of the proposed intracellular activation pathway. (a) The stable, cold structure. (b) A hydrophobic cluster in the CT domain is destabilized by heat. (c) This allows a new cluster to form between the CT and Linker domains. This pulls the Linker domain away from the VBP, (d) breaking hydrogen bonds between the Linker and S2-S3 link, and opening the VBP. (e) The lipid is free to move around in the VBP and it eventually leaves. (f) A new HB forms between S4 and S5, pulling S6 away from the ion channel and opening the gate.

4. Conclusions

In this study, all-atom simulations of TRPV1 are conducted at 290 and 350 K in an attempt to uncover the mechanisms and structures granting it its remarkable thermal sensitivity. The previously suggested mechanisms in the extracellular pore domain, i.e., the destabilization of the hydrophobic cluster and the subsequent release of the extracellular selectivity filter, are reproduced. Then, we investigate the interactions between the CT and linker domains as well as the role of the lipids embedded in the vanilloid binding pocket. While the long, relatively unstructured CT loop precludes strong, deterministic conclusions, we integrate our findings in order to propose the intracellular thermal sensation pathway shown in Fig. 10 and summarized below.

[CTL.ii, Fig. 10(b)] A cluster of residues in the long CT loop is destabilized by heat. [CTL.iii, Fig. 10(c)] This allows key residues (Arg739, Arg743) to form a new, hydrogen bound cluster with the adjacent one-turn helix in the linker domain (383 to 389). [CTL.iv, Fig. 10(c)] the new cluster pulls this small helix away from the central axis of TRPV1, [CTL.v, Fig. 10(c)] which in turn pulls on a linker helix above the vanilloid binding pocket through the Ser394 - Thr389 hydrogen bond. [VBP.i, Fig. 10(d)] As the linker helix is displaced, a key residue in its attached loop, Arg409, is pulled away from the S1-S4 structure, breaking the Arg409 - Asp509 hydrogen bond and allowing the linker loop to reposition away from the vanilloid binding pocket and form a new bond with Glu692 or a cluster with other residues in the linker loop. (VBP.iii, Fig. 10(d)) This allows Asp509 to reposition, forming a new hydrogen bond with Tyr495, which moves the S2-S3 linking loop away from the vanilloid binding pocket as well. In combination, (VBP.i) and (VBP.iii) open up the vanilloid binding pocket which frees the phosphatidylinositol lipid embedded therein. (VBP.iv, Fig. 10(e)) Once free, the lipid is displaced or completely ejected, breaking the hydrogen bonds between the lipid and Arg557/Glu570. (VBP.v, Fig. 10(f)) Afterwards, these residues form a new hydrogen bond with each other, pulling the S4-S5 linker away from the central axis and encouraging the dilation of the intracellular gate.

We must note, however, that the correlation between the changes in the CTL region and the changes in the VBP are very weak. Indeed, the large flexibility of the CTL region precludes strong correlations, even for the intra CTL changes. Additionally, the linker loops above the VBP form a number of different hydrogen bound structures, creating large variance to the statistical analysis of changes therein. Indeed, its possible that multiple configurational pathways exist which integrate, e.g., the configuration changes noted at the N-terminal of the CT domain (CTL.i) and the hybridization of the TRP and S6 helices (VBP.ii). Finally, the lack of simulations at physiological temperatures, e.g., at 310 and 330 K, which complement our low (290 K) and high (350 K) temperature simulations means that we cannot analyze the role of temperature in preventing the escape of TRPV1 at low temperatures from its initial meta-stable structures and hydrogen bonds which should not exist or form stable ones at high temperatures which should exist. While we have tried to tie our results to the literature, thermodynamic considerations, and physically in order to focus on those hydrogen bonds and structures which actually respond to heat, some caution should be applied when analyzing our results, particularly the hydrogen bonding analyses. Indeed, while the literature and our own results strongly support many of the steps along this pathway, the evidence for some of them is limited. For these reasons the intracellular thermosensation pathway requires further examination. For example, experimental researchers could mutate key residues in the CT-linker cluster (e.g., Arg739 and Arg743) or connecting helices (e.g., Asp388 and Thr393). Within our model of the pathway, this should influence temperature sensitivity without affecting vanilloid sensitivity.

Regardless, we have still supported and explored novel hypotheses surrounding the intracellular pathway. Primarily, we support the recent hypothesis that heat ejects lipids from the vanilloid binding pockets (Gao et al., 2016). Additionally, we support the existence of thermally sensing residues in the CT (Arg739 to Arg743) (Raymond et al., 2014) and throughout the linker domain (Wen et al., 2016; Zheng and Qin, 2015).

Unfortunately, the complete opening of TRPV1 is not achieved in our simulations, and the intracellular gate remains closed. This makes it impossible to definitively connect the intracellular or extracellular pathways to the dilation of the intracellular gate. With trajectories in the microsecond domain, thermally induced opening may be achieved, which would allow researchers to extend grounded hypothesis connecting changes in the vanilloid binding pocket, CT, and linker domains to the thermally induced opening of the intracellular gate. However, current computational limits prevent this goal from being achieved within a reasonable time frame. Alternatively, the TRPV1 structure may still require modification. For example, recent simulations suggest that non-polar cavities in TRPV1 must be hydrated for thermally induced opening to occur (Kasimova et al., 2017). Future simulations should address these issues for more a comprehensive analysis.

Acknowledgments

This work was supported by the NSF program on Thermal Transport and Processes (Award No. CBET1332807), and it used the computational resources of the Oak Ridge Leadership Computing Facility at the Oak Ridge National Laboratory, which is supported by the Office of Science of the U.S. Department of Energy under Contract No. DE-AC05-00OR22725. It employed additional computing resources through the DOE National Energy Research Scientific Computing Center (Office of Science, Contract No. DE-AC02-05CH11231).

Supplementary material

Supplementary material associated with this article can be found, in the online version, at doi:10.1016/j.jtbi.2018.02.004.

References

Bae, C., Anselmi, C., Kalia, J., Jara-Oseguera, A., Scheieters, C.D., Krepkiy, D., Lee, C.W., Kim, E.-H., Kim, J.I., Faraldo-Gómez, J.D., Swartz, K.J., 2016. Structural insights into the mechanism of activation of the TRPV1 channel by a membrane-bound tarantula toxin. Elife 5, e11273. doi:10.7554/eLife.11273.

Brauchi, S., Orta, G., Mascayano, C., Salazar, M., Raddatz, N., Urbina, H., Rosenmann, E., Gonzalez-Nilo, F., Latorre, R., 2007. Dissection of the componptents for PIP_2 activation and thermosensation in TRP channels. Proc. Nat. Acad. Sci. USA 104, 10246–10251. doi:10.1073/pnas.0703420104.

Brauchi, S., Orta, G., Salzar, M., Rosenmann, E., Latorre, R., 2006. A hot-sensing cold receptor: C-terminal domain determines thermosensation in transient receptor potential channels. J. Neurosci. 26, 4835–4840. doi:10.1523/JNEUROSCI.5080-05.2006.

Cao, E., Liao, M., Cheng, Y., Julius, D., 2013. TRPV1 structures in distinct conformations reveal mechanisms of activation. Nature 504, 113. doi:10.1038/nature12823.

Caterina, M., Rosen, T., Tominaga, M., Brake, A., Julius, D., 1999. A capsaicin-receptor homologue with a high threshold for noxious heat. Nature 398, 436–441. doi:10.1038/18906.

Caterina, M., Schumacher, M., Tominaga, M., Rosen, T., Levine, J., Julius, D., 1997. The capsaicin receptor: a heat-activated ion channel in the pain pathway. Nature 389, 816–824. doi:10.1038/39807.

Catterall, W., 2012. Voltage-gated sodium channels at 60: structure, function and pathophysiology. J. Physiol. 590, 2577–2589. doi:10.1113/jphysiol.2011.224204.

Catterall, W.A., 2010. Ion channel voltage sensors: structure, function, and pathophysiology. Neuron 67, 915–928. doi:10.1016/j.neuron.2010.08.021.

Chugunov, A., Volynsky, P., Krylov, N., Nolde, D., Efremov, R., 2016. Temperature-sensitive gating of TRPV1 channel as probed by atomistic simulations of its trans- and juxtamembrane domains. Sci. Rep. 6, 33112. doi:10.1038/srep33112.

Clapham, D., 2003. Trp channels as cellular sensors. Nature 426, 517–524. doi:10.1038/nature02196.

Clapham, D., Miller, C., 2011. A thermodynamic framework for understanding temperature sensing by transient receptor potential (trp) channels. Proc. Natl. Acad. Sci. USA 108, 19492. doi:10.1073/pnas.1117485108.
Darden, T., York, D., Pedersen, L., 1993. Particle mesh ewald: an nâog(n) method for ewald sums in large systems. J. Chem. Phys. 98, 10089. doi:10.1063/1.464397.
Dhaka, A., Viswanath, V., Patapoutian, A., 2006. Trp ion channels and temperature sensation. Annu. Rev. Nerosci. 29, 135. doi:10.1146/annurev.neuro.29.051605.112958.
Dolinsky, T., Nielsen, J., MMcCammon, J., Baker, N., 2004. Pdb2pqr: an automated pipeline for the setup, execution, and analysis of poisson-boltzmann electrostatics calculations. Nucleic Acids Res. 32, W665–W667. doi:10.1093/nar/gkh381.
Feller, S., Zhang, Y., Pastor, R., 1995. Constant pressure molecular dynamics simulation: the Langevin piston method. J. Chem. Phys. 103, 4613. doi:10.1063/1.470648.
Gao, Y., Cao, E., Julius, D., Cheng, Y., 2016. TRPV1 structures in nanodiscs reveal mechanisms of ligand and lipid action. Nature 534, 347. doi:10.1038/nature17964.
Gaudet, R., 2008. A primer on ankyrin repeat function in TRP channels and beyond. Mol. Biosyst. 4, 372–379. doi:10.1039/b801481g.
Glykos, N., 2006. Carma: a molecular dynamics analysis program. J. Comput. Chem. 27, 1765. doi:10.1002/jcc.20482.
Grandl, J., Kim, S.E., Uzzell, V., Bursulaya, B., petrus, M., Bandell, M., Patapoutian, A., 2010. Temperature-induced opening of TRPV1 ion channel is stabilized by the pore domain. Nat. Neuro. 13, 708. doi:10.1038/nn.2552.
Gunthhorpe, M., Szallasi, A., 2008. Peripheral TRPV1 receptors as targets for drug development: new molecules and mechanisms. Curr. Pharm. Des. 14, 32–41. doi:10.2174/138161208783330754.
Hu, H., Grandl, J., Bandell, M., Petrus, M., Patapoutian, A., 2009. Two amino acid residues determine 2-APB sensitivity of the ion channels TRPV3 and TRPV4. Proc. Natl. Acad. Sci. USA 106 (5), 1626–1631. doi:10.1073/pnas.0812209106.
Huang, J., MacKerell, A., 2013. CHARMM36 all-atom additive protein force field: validation based on comparison to NMR data. J. Comput. Chem. 34, 2135–2145. doi:10.1002/jcc.23354.
Hui, K., Liu, B., Qin, F., 2003. Capsaicin activation of the pain receptor, VR1: multiple open states from both partial and full binding. Biophys. J. 84, 2957.
Humphrey, W., Dalke, A., Schulten, K., 1996. Vmd: visual molecular dynamics. J. Mol. Graphics 14, 33–38. doi:10.1016/0263-7855(96)00018-5.
Jara-Oseguera, A., Bae, C., Swartz, K.J., 2016. An external sodium ion binding site controls allosteric gating in TRPV1 channels. Elife 5, e13356. doi:10.7554/eLife.13356.
Jendryke, T., Prochazkova, M., Hall, B.E., Nordmann, G.C., Schladt, M., Milenkovic, V.M., Kulkarni, A.B., Wetzel, C.H., 2016. TRPV1 function is modulated by cdk5-mediated phosphorylation: insights into the molecular mechanism of nociception. Sci. Rep. 6, 22007. doi:10.1038/srep22007.
Jensen, M.O., Jogini, V., Borhani, D.W., Leffler, A.E., Dror, R.O., Shaw, D.E., 2012. Mechanism of voltage gating in potassium channels. Science 336, 229. doi:10.1126/science.1216533.
Jiang, H., Li, C., Huang, X., 2013. Actuators based on liquid crystalline elastomer materials. Nanoscale 5, 5225–5240. doi:10.1039/c3nr00037k.
Jolliffe, I., 2002. Principle Component Analysis, second ed. Springer.
Jordt, S., Tominaga, M., Julius, D., 2000. Acid potentiation of the capsaicin receptor determined by a key extracellular site. Proc. Natl. Acad. Sci. USA 97, 8134–8139. doi:10.1073/pnas.100129497.
Jorgensen, W., Chandrasekhar, J., Madura, J., Impey, R., Klein, M., 1983. Comparison of simple potential functions for simulating liquid water. J. Chem. Phys. 79, 926–935. doi:10.1063/1.445869.
Karashima, Y., Talavera, K., Everaerts, W., Janssens, A., Kwan, K., Bennekens, R., Nilius, B., Voets, T., 2009. Trpa1 acts as a cold sensor in vitro and in vivo. Proc. Natl. Acad. Sci. USA 106, 1273–1278. doi:10.1073/pnas.0808487106.
Kasimova, M., Yazici, A., Granata, D., Klein, M., Rohacs, T., Carnevale, V., 2017. TRPV1 activation relies on hydration/dehydration of nonpolar cavities. bioRxiv.
Kaufmann, K., Lemmon, G., Deluca, S., Sheehan, J., Meiler, J., 2010. Practically useful: what the rosetta protein modeling suite can do for you. Biochemistry 49, 2987. doi:10.1021/bi902153g.
Klauda, J., Venable, R., Freites, J., O'connor, J., Tobias, D., Mondragon-Ramirez, C., Vorobyov, I., MacKerell, A., Jr., R.P., 2010. Update of the CHARMM all-atom additive force field for lipids: validation on six lipid types. J. Phys. Chem. B 114, 7830–7843. doi:10.1021/jp101759q.
Liao, M., Cao, E., Julius, D., Cheng, Y., 2013. Structure of the TRPV1 ion channel determined by electron cryo-microscopy. Nature 504, 107. doi:10.1038/nature12822.
Lomize, M., Lomize, A., Pogozheva, I., Mosberg, H., 2006. OPM: orientations of proteins in membranes database. Bioinformatics 22, 623–625.
Martyna, G., Tobias, D., Klein, M., 1994. Constant pressure molecular dynamics algorithms. J. Chem. Phys. 101, 4177. doi:10.1063/1.467468.
Myers, B.R., Bohlen, C.J., Julius, D., 2008. A yeast genetic screen reveals a critical role for the pore helix domain in TRP channel gating. Neuron 58 (3), 362–373. j.neuron.2008.04.012
Nilius, B., 2007. Trp channels in disease. Biochem. Biophys. Acta 1772, 8005–8812. doi:10.1016/j.bbadis.2007.02.002.
Nilius, B., 2013. Transient receptor potential TRP channels as therapeutic drug targets: next round!. Curr. Top. Med. Chem. 13, 244–246. doi:10.2174/15680266112129990085.
Nilius, B., Appendino, G., Owsianik, G., 2012. The transient receptor potential channel trpa1: from gene to pathophysiology. Pflugers Arch. 464, 425–458. doi:10.1007/s00424-012-1158-z.
Nilius, B., Voets, T., Peters, J., 2005. Trp channels in disease. Sci. STKE 2005, re8. doi:10.1126/stke.2952005re8.
Phillips, J.C., Braun, R., Wang, W., Gumbart, J., Tajkhorshid, E., Villa, E., Chipot, C., Skeel, R.D., Kale, L., Schulten, K., 2005. Scalable molecular dynamics with NAMD. J. Comp. Chem. 26, 1781–1802. doi:10.1002/jcc.20289.
Raymond, K.A., Twomey, E.C., Wei, Y., 2014. Characterization of temperature-sensing and PIP_2-regulation of TRPV1 ion channel at the c-terminal domain using nmr spectroscopy and molecular dynamics simulations. J. Integr. OMICS 4, 79. doi:10.5584/jiomics.v4i2.158.
Ryu, S., Liu, B., Yao, J., Fu, Q., Qin, F., 2007. Uncoupling proton activation of vanilloid receptor TRPV1. J. Neurosci. 27 (47), 12797–12807. doi:10.1523/JNEUROSCI.2324-07.2007.
Schlitter, J., 1993. Estimation of absolute and relative entropies of macromolecules using the covariance matrix. Chem. Phys. Lett. 215 (6), 617. doi:10.1016/0009-2614(93)89366-P.
Story, G., Peier, A., Reeve, A., Eid, S., Mosbacher, J., Hricik, T., Early, T., Hergarden, A., D.A., A., S.W, H., McIntyre, P., Jegla, T., S., B., A., P., 2003. ANKTM1, a trp-like channel expressed in nociceptive neurons is activated by cold temperatures. Cell 112, 819–829. doi:10.1016/S0092-8674(03)00158-2.
Tominaga, M., Caterina, M., Malmberg, A., Rosen, T., Gilbert, H., Skinner, K., Raumann, B., Basbaum, A., Julius, D., 1998. The cloned capsaicin receptor integrates multiple pain-producing stimuli. Neuron 21, 531–543. doi:10.1016/S0896-6273(00)80564-4.
Voets, T., Droogmans, G., Wissenbach, U., Janssens, A., Flockerzi, V., Nilius, B., 2004. The principle of temperature-dependent gating in cold- and heat-sensitive TRP channels. Nature 430, 748–754. doi:10.1038/nature02732.
Voets, T., Talavera, K., Owsianik, G., Nilius, B., 2005. Sensing with TRP channels. Nat. Chem. Biol. 1, 85–92. doi:10.1038/nchembio0705-85.
Ware, T., Hearon, K., Lonnecker, A., Wooley, K., Maitland, D.J., Voit, W., 2012. Triple-shape memory polymers based on self-complementary hydrogen bonding. Macromolecules 45, 1062–1069. doi:10.1021/ma202098s.
Wen, H., Qin, F., Zheng, W., 2016. Toward elucidating the heat activation mechanism of the TRPV1 channel gating by molecular dynamics simulation. Proteins 84, 1938. doi:10.1002/prot.25177.
Wen, H., Zheng, W., 2018. Decrypting the heat activation mechanism of trpv1 channel by molecular dynamics simulation. Biophys. J. 114, 40.
Yang, F., Cui, Y., Wang, K., Zheng, J., 2010. Reply to Yao et al.: Is the pore turret just thermoTRP channelsâ appendix? PNAS 107, E126–E127. doi:10.1073/pnas.1008504107.
Yang, F., Cui, Y., Wang, K., Zheng, J., 2010. Thermosensitive TRP channel pore turret is part of the temperature activation pathway. PNAS 107, 7083–7088. doi:10.1073/pnas.1000357107.
Yang, F., Xiao, X., Cheng, W., Yang, W., Yu, P., Song, Z., Yarov-Yarovoy, V., Zheng, J., 2015. Structural mechanism underlying capsaicin binding and activation of the trpv1 ion channel. Nat. Chem. Bio. 11, 518.
Yao, J., Liu, B., Qin, F., 2010. Pore turret of thermal TRP channels is not essential for temperature sensing. PNAS 107, E125. doi:10.1073/pnas.1008272107.
Yao, J., Liu, B., Qin, F., 2011. Modular thermal sensors in temperature-gated transient receptor potential (TRP) channels. Proc. Natl. Acad. Sci. USA 108, 11109–11114. doi:10.1073/pnas.1105196108.
Zhang, L., Hermans, J., 1996. Hydrophilicity of cavities in proteins. Proteins Struct. Funct. Genet. 24, 433. doi:10.1002/(SICI)1097-0134(199604)24:4⟨433::AID-PROT3⟩3.0.CO;2-F.
Zheng, W., Qin, F., 2015. A combined coarse-grained and all-atom simulation of TRPV1 channel gating and heat activation. J. Gen. Phys. 145, 443. doi:10.1085/jpg.201411335.